

The hyperfine structure of $^{129}\text{I}_2$ and $^{127}\text{I}^{129}\text{I}$ in the $\text{B}^3\Pi_{0_u^+}-\text{X}^1\Sigma_g^+$ band system

E. J. SALUMBIDES[†], K. S. E. EIKEMA[†], W. UBACHS[†],
U. HOLLENSTEIN^{†‡}, H. KNÖCKEL^{*§} and E. TIEMANN[§]

[†]Laser Centre Vrije Universiteit, De Boelelaan 1081, 1081 HV Amsterdam, The Netherlands

[‡]Laboratorium für Physikalische Chemie, ETH Zürich, CH-8093 Zürich, Switzerland

[§]Institut für Quantenoptik, Universität Hannover, Welfengarten 1, 30167 Hannover, Germany

(Received 1 March 2006; in final form 19 April 2006)

In a double saturation spectroscopy experiment, using the radiation from one single frequency cw laser, the spectra of $^{129}\text{I}_2$ and $^{127}\text{I}^{129}\text{I}$ from one saturation setup were recorded simultaneously and with respect to the spectrum of $^{127}\text{I}_2$ from another setup while tuning the laser. The hyperfine patterns of $^{129}\text{I}_2$ and $^{127}\text{I}^{129}\text{I}$ were analysed to determine the nuclear electric quadrupole interaction and the nuclear spin–rotation interaction parameters. Models are presented describing the observations and giving reliable predictions for the hyperfine parameters of all isotopomers.

1. Introduction

The visible $\text{B}^3\Pi_{0_u^+}-\text{X}^1\Sigma_g^+$ system of molecular $^{127}\text{I}_2$ is widely used as a convenient reference spectrum for spectroscopic purposes, because the experimental setups to create iodine spectra are simple and the precision of 10^{-7} or sometimes better is sufficient for many purposes. Spectra for comparison with observed ones are available in the form of the iodine atlas by Gerstenkorn and Luc [1] for linear absorption spectra, or from Doppler free spectroscopy in the atlas by Katô *et al.* [2].

Recently, some of the present authors were involved in proposing model descriptions for the rovibrational [3] and for the hyperfine structure [4] of the $\text{B}^3\Pi_{0_u^+}-\text{X}^1\Sigma_g^+$ system of $^{127}\text{I}_2$. Combining such models it is possible to identify observed iodine spectral lines and to predict their frequencies to better than 2 MHz in large frequency ranges. Both models have also been included in a program to predict frequencies of iodine lines, which then can be used for calibration [5]. The models are based on the data available from literature (see [4]) at that time, which put restrictions on the ranges of validity, e.g. $v' = 43$ being the uppermost vibrational level in the B state.

In the meantime, Chen *et al.* [6] have reported measurements beyond $v' = 42$ to higher v' in the B state for the isotopomer $^{127}\text{I}_2$. They also applied successfully a different approach to the description of the rovibrational dependence of the hyperfine parameters, which accounts for the dependence of the hyperfine interactions on the internuclear distance averaged over the vibrational motion. In that framework observations close to the dissociation limit could be modelled by including distinct electronic states sharing the same asymptote, and the resulting perturbations in the upper levels of the $\text{B}^3\Pi_{0_u^+}$ [7].

Thus, new data are available offering the possibility to extend models of the hyperfine structure in the B–X system. The ultimate goal of the present study is, however, to help provide an accurate spectroscopic frequency standard based on the $\text{B}^3\Pi_{0_u^+}-\text{X}^1\Sigma_g^+$ band system for the three iodine molecular isotopomers; such a reference standard would be a factor of three more dense than the one solely based on the $^{127}\text{I}_2$ species. In addition, more reliable information on the rovibronic structure of the excited $\text{B}^3\Pi_{0_u^+}$ state for those isotopomers is obtained, for the purpose of a better determination of the Born–Oppenheimer corrections, which could not be determined sufficiently precise in a previous paper [3].

The $^{129}\text{I}_2$ and $^{127}\text{I}^{129}\text{I}$ molecules have been studied previously, although in much less detail than the main $^{127}\text{I}_2$ isotopomer. Cerny *et al.* presented an analysis

*Corresponding author. Email: Knoeckel@iqo.uni-hannover.de

of the rotational structure of the B–X system for both ^{129}I -containing isotopomers, based on a laser-induced fluorescence Fourier-transform spectroscopic study [8]. Previously, information on two excited vibrational levels in the B state of the $^{127}\text{I}^{129}\text{I}$ isotopomer had been obtained [9], while also the hyperfine structure near 633 nm had been unravelled [10]. High precision splittings of few lines around 633 nm are tabulated in [11]. Recently, in a study focusing on Raman lasing at 532 nm in I_2 some accurate information on the level structure of $^{129}\text{I}_2$ and $^{127}\text{I}^{129}\text{I}$ was obtained [12].

In the present paper we report on systematic investigations of iodine spectra of the isotopomers $^{129}\text{I}_2$ and $^{127}\text{I}^{129}\text{I}$ covering a set of vibrational levels in the B state between $v' = 8$ and $v' = 20$ and in the ground state between $v'' = 0$ and $v'' = 5$. In these experiments hyperfine structures of many lines of the homonuclear $^{129}\text{I}_2$ and the heteronuclear $^{127}\text{I}^{129}\text{I}$ isotopomer were recorded simultaneously with $^{127}\text{I}_2$ for calibration in a double spectrometer.

The paper is organized as follows: in the next section we shall give a short outline of the experiment. A section discussing the description of the hyperfine structure follows, after which the measurements and the results on the different isotopomers will be presented. In the analysis section, improved model descriptions for the hyperfine interactions are presented, which, for easy application in prediction of transition frequencies, are based on the simple Dunham series approach like in [4]. While in [4] no data of the

isotopomers $^{129}\text{I}_2$ and $^{127}\text{I}^{129}\text{I}$ had been included, the models presented here have been extended for use with all isotopomers. A discussion and conclusion will summarize the achievements of the paper.

2. Experimental

A schematic layout of the setup is shown in figure 1. A stabilized cw ring-dye-laser (Spectra Physics 380D) is used as the radiation source. The dye laser is operated with Rhodamine 6G dye to access the wavelength range of 573 to 583 nm, while Rhodamine B dye is used for the range 610 to 615 nm and for some measurements near 633 nm.

Two saturated absorption setups allow for the simultaneous recording of the spectra obtained from a vapour cell containing the $^{129}\text{I}_2$ and $^{127}\text{I}^{129}\text{I}$ isotopomers with that of the main $^{127}\text{I}_2$ isotopomer in another cell. By means of this double saturation setup, the spectra of the $^{129}\text{I}_2$ and $^{127}\text{I}^{129}\text{I}$ isotopomers can be calibrated on an absolute scale using the $^{127}\text{I}_2$ resonances that have been measured at high accuracy before [13, 14]. Although for the present article, focusing on the hyperfine structure of the $^{129}\text{I}_2$ and $^{127}\text{I}^{129}\text{I}$ molecules, a relative frequency calibration would suffice, the data on the ^{129}I containing species are calibrated on an absolute scale in view of a subsequent paper on a description of the rovibronic structure of the iodine molecule for all three isotopomers.

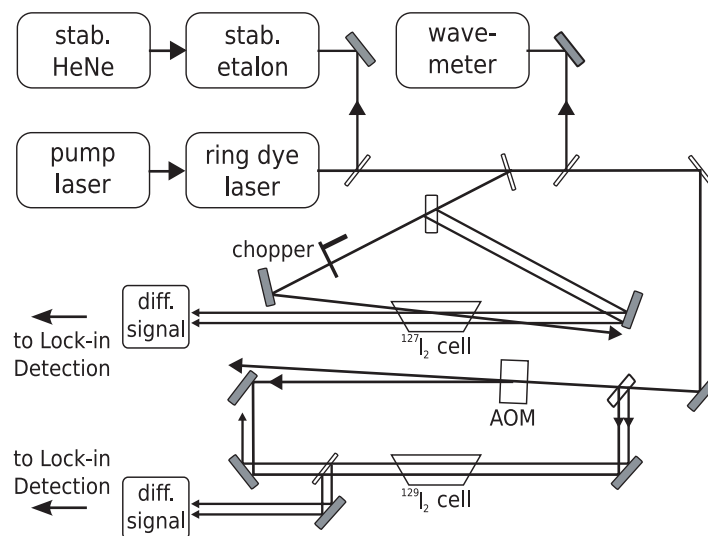


Figure 1. The experiment consists of parallel saturation spectroscopy measurements on two vapour cells, one containing $^{129}\text{I}_2$ (and $^{127}\text{I}^{129}\text{I}$ and traces of $^{127}\text{I}_2$) and the other containing $^{127}\text{I}_2$. The positions of the $^{129}\text{I}_2$ and $^{127}\text{I}^{129}\text{I}$ resonances are determined relative to the position of $^{127}\text{I}_2$ lines by means of a stabilized étalon.

A 10 cm vapour cell containing 100% $^{127}\text{I}_2$ is used in one of the saturation setups, identical to the one used in the previous studies discussed in [13] and [14]. Differential absorption is monitored, where one of the probe beams is crossed at a slight angle (<14 mrad) with the saturation beam. The saturating beam is modulated by a mechanical chopper at around 700 Hz and lock-in signal detection is employed. The $^{127}\text{I}_2$ cell is used at room temperature vapour pressure.

A 5 cm cell containing $^{129}\text{I}_2$ and $^{127}\text{I}^{129}\text{I}$ is used in the other saturation setup. The pump-offset saturation spectroscopy technique [15, 16] is used to maximize the signal detection sensitivity. The first-order diffraction beam from an acousto-optic modulator (AOM) shifted by +75 MHz is used as the saturating beam. As a consequence of the 75 MHz frequency offset of the saturating beam with respect to the probe beams, the saturation resonances are shifted by 37.5 MHz from the real line positions [15, 16]. Differential absorption signals were acquired, with one of the probe beams overlapped collinearly with the saturating beam. A 50 kHz modulation was imposed on the amplitude of the saturating beam and the saturation signal is retrieved by lock-in detection. The inherent sensitivity of the pump-offset technique combined with the fast modulation of the AOM results in a high detection sensitivity. With such a scheme, we could detect the strong transitions of the $^{127}\text{I}_2$ molecules that are also present in trace amounts inside this cell. These weak $^{127}\text{I}_2$ signals are compared to that obtained from the parallel $^{127}\text{I}_2$ saturation setup in order to check for possible frequency shifts between the two saturation setups.

A wavemeter is used to coarsely tune the laser to the resonances. Relative frequency calibrations are carried out by employing the transmission peaks of a 50 cm Fabry–Pérot étalon. The étalon temperature and pressure is stabilized and its length is actively locked to the wavelength of a Zeeman-stabilized He:Ne laser. The étalon free spectral range FSR is measured at the start of every measurement session, which has a typical value of 148.96(1) MHz with small day to day variations. For the absolute frequency calibration of the $^{129}\text{I}_2$ and $^{127}\text{I}^{129}\text{I}$ lines a nearby lying $^{127}\text{I}_2$ line was chosen as reference, which has been measured previously in [13, 14]. Since the largest separation was less than 30 étalon fringes, this procedure results in a sub-MHz frequency uncertainty, in addition to the uncertainty of the $^{127}\text{I}_2$ calibration, which is typically 1 MHz (1σ). The relative frequency scale is mainly determined by some remaining nonlinearity of the laser scan, that is left over after a computerized linearization procedure; it is also of sub-MHz order.

3. Hyperfine structure

3.1. Basic considerations

The hyperfine structure of the iodine molecule is described by an effective Hamiltonian [17]:

$$H_{\text{hfs,eff}} = H_{\text{NEQ}} + H_{\text{SR}} + H_{\text{SS}} + H_{\text{TS}}. \quad (1)$$

H_{NEQ} , H_{SR} , H_{SS} and H_{TS} represent the (effective) nuclear electric quadrupole, the nuclear spin–rotation, the scalar nuclear spin–spin and the tensorial nuclear spin–spin interactions. The matrix elements of each of these terms can be separated into a product of a geometrical factor g_i and a hyperfine parameter, i.e. eqQ , C , δ or d :

$$\begin{aligned} \langle \alpha', F | H_{\text{hfs,eff}} | \alpha, F \rangle \\ = eqQ \cdot g_{eqQ} + C \cdot g_{\text{SR}} + \delta \cdot g_{\text{SS}} + d \cdot g_{\text{TS}}. \end{aligned} \quad (2)$$

α represents a set of quantum numbers characterizing the molecular level, which will be specified later, and F is the total angular momentum. The g_i are functions of appropriate angular momentum quantum numbers of the system, and can be calculated with spherical tensor algebra. The hyperfine parameters are usually determined experimentally from the measured hyperfine structure of a rovibrational transition.

For calculation of the factors g_i different coupling schemes were applied. The homonuclear molecules $^{127}\text{I}_2$ and $^{129}\text{I}_2$ are characterized by a wave function $|\Omega v(I_1 I_2) J J F M_F\rangle$ [17]. The two nuclear spins \mathbf{I}_1 and \mathbf{I}_2 couple to a total nuclear spin \mathbf{I} , which is then coupled with the rotational angular momentum \mathbf{J} to give a total angular momentum \mathbf{F} . Ω is the projection of the total electronic angular momentum on the internuclear axis and characterizes the electronic state, while v is the vibrational quantum number. Here the computer code, described in more detail in [18], was applied.

For the spectra of the heteronuclear species a coupling scheme corresponding to the notation $|\Omega v(J I_1) F_1 I_2 F M_F\rangle$ is used, and all simplifications due to symmetry like in the homonuclear case are absent. Moreover, for each nucleus appropriate hyperfine parameters must be used, which means $eqQ^{(127)}$, $eqQ^{(129)}$, $C^{(127)}$, $C^{(129)}$, ... values for each electronic state. An appropriate computer code was available. The corresponding matrix elements are taken from [19]. The nuclear spin–spin interactions are not included. Due to its small contribution of not more than 400 kHz to the hyperfine splitting and in view of the limited signal-to-noise ratio in our spectra

this neglect does not change the results on the molecular parameters.

Providing the hyperfine parameters for both states, and the rotational angular momentum quantum number J'' and J' , the computer codes calculate the hyperfine splitting frequencies and also relative intensities of the hyperfine lines, using for the dipole matrix element the eigenvectors determined during the diagonalization of the hyperfine interaction matrix for each state, extending the rotational space up to $\Delta J = 0, \pm 2$.

It was verified that the code for heteronuclear species gives the same results, within numerical accuracy, as the code for the homonuclear species for situations where the results should coincide.

3.2. Rovibrational dependence of the hyperfine parameters

The hyperfine parameters are products of an electronic part and the expectation value of the corresponding nuclear moment. The electronic part depends on the vibrational and rotational quantum numbers of the levels involved. The form for the rovibrational dependence is based on that used in [4]. For convenience we give a short outline of the nomenclature.

The functional forms of the effective hyperfine parameters were explicitly given by Broyer *et al.* [17]. Following their paper we use for both the ground state $X^1\Sigma_g^+$ and the excited state $B^3\Pi_{0g^+}$, which are $\Omega=0$ states, representations of the form:

$$\chi(v, J) = \chi^{(1)}(v, J) + \sum_p \frac{\chi^{(p)}(v, J)}{\Delta E_{v, v_p}^J} \cdot \langle v | v^{(p)} \rangle, \quad (3)$$

where χ stands for eqQ , C , δ or d . $\chi^{(1)}$ is the first-order contribution of the discussed electronic state (**B** or **X**) and $\chi^{(p)}$ is a second-order contribution from a perturbing state p with energy difference $\Delta E_{v, v_p}$ between the levels (v, J) and (v_p, J) and the overlap integral $\langle v | v^{(p)} \rangle$ of the two vibrational states. This form is a simple approximation for the case where the electronic matrix element will have only a weak dependence on the nuclear separation. $\chi^{(1)}$ is the expectation value of the generally R -dependent interaction for the specific rovibrational state (v, J) . This is represented here in the form of a Dunham series in v and J ,

$$\chi(v, J) = \sum_{l, k} \chi_{lk} \cdot (v + 1/2)^l \cdot [J(J + 1)]^k. \quad (4)$$

Few members of this series are usually sufficient for describing the set of experimental data. The coefficients χ_{lk} can also be related to the potential of the electronic state, and a power expansion of χ with the internuclear distance R can be derived. Such an approach was recently used by Chen *et al.* [6, 7] and earlier by Spirko and Blabla [20]. For the sake of simplicity of recalculation by other researchers, however, we shall follow the Dunham approach.

The sum over the perturbing states contains two different categories: in the first one, where the electronic state p is close by, the energy denominator plays an important role in the functional form of the parameter. In the second one, the perturbing state is so far away that its contribution does not vary significantly with v_p , so that this part is barely distinguishable from the functional form of $\chi^{(1)}(v, J)$. In the iodine molecule the states mainly perturbing the $X^1\Sigma_g^+$ share the same atomic asymptote as **X** and are weakly bound. Thus the energy denominator can be approximated by $\Delta E_{v, v_p}^J \approx E_{v, J} - \bar{E}_p(3/2, 3/2)$, where \bar{E}_p is an average of the perturbing levels and will have a value close to that of the atomic asymptote $^2P_{3/2} + ^2P_{3/2}$. Also the overlap integral $\langle v | v_p \rangle$ will not vary strongly with v_p in this case, because the part of the wave function for small nuclear separation will almost stay constant while varying v_p up to the dissociation limit, so that $\chi^{(p)} \cdot \langle v | v_p \rangle$ can be approximated by a short Dunham expansion.

Quite similarly we approximate the functional form of the hyperfine parameters of the **B** state, the dissociation asymptote now being $^2P_{1/2} + ^2P_{3/2}$ of iodine, and again we introduce as an average energy for the perturbing state $\bar{E}_p(1/2, 3/2)$. In total, we get for the nuclear electric quadrupole interaction ($\chi = eqQ$) and for the nuclear spin-rotation interaction ($\chi = C$) the formula

$$\chi(v, J) = \sum_{lk} \chi_{lk}^{(1)} \cdot (v + 1/2)^l \cdot [J(J + 1)]^k + \sum_p \frac{\sum_{lk} \chi_{lk}^{(p)} \cdot (v + 1/2)^l \cdot [J(J + 1)]^k}{E_{v, J} - \bar{E}_p}. \quad (5)$$

\bar{E}_p stands for $\bar{E}_p(3/2, 3/2)$ or $\bar{E}_p(1/2, 3/2)$.

The derivation in [17] of the second-order contributions of the scalar and tensorial spin-spin interactions, i.e. the parameters δ and d , reveals that they have common contributions due to the perturbing states involved. Here, we have to consider $\Omega_p = 0$ and 1. In the former case, both contributions differ in sign, in the

latter case by a factor of 1/2. This gives the following formulae for the two interaction parameters

$$\begin{aligned} \delta = & \sum_{lk} \delta_{lk} \cdot (v+1/2)^l \cdot [J(J+1)]^k \\ & + \frac{\sum_{lk} \chi_{lk}^{(\Omega=0)} \cdot (v+1/2)^l \cdot [J(J+1)]^k}{E_{v,J} - \bar{E}_{\Omega=0}} \\ & + \frac{\sum_{lk} \chi_{lk}^{(\Omega=1)} \cdot (v+1/2)^l \cdot [J(J+1)]^k}{E_{v,J} - \bar{E}_{\Omega=1}} \\ & + \eta \exp\left(-\frac{(E_{v,J} - E_c)^2}{W}\right), \end{aligned} \quad (6)$$

$$\begin{aligned} d = & \sum_{lk} d_{lk} \cdot (v+1/2)^l \cdot [J(J+1)]^k \\ & - \frac{\sum_{lk} \chi_{lk}^{(\Omega=0)} \cdot (v+1/2)^l \cdot [J(J+1)]^k}{E_{v,J} - \bar{E}_{\Omega=0}} \\ & + \frac{1}{2} \frac{\sum_{lk} \chi_{lk}^{(\Omega=1)} \cdot (v+1/2)^l \cdot [J(J+1)]^k}{E_{v,J} - \bar{E}_{\Omega=1}} \\ & + \frac{\eta}{2} \exp\left(-\frac{(E_{v,J} - E_c)^2}{W}\right), \end{aligned} \quad (7)$$

where the second and third terms in each equation describe the effective perturbations due to $\Omega=0$ states and $\Omega=1$ states. The fourth terms in both equations were introduced in [4] as a simplified Gaussian representation with an amplitude η and a width of $W^{1/2}$ for the local perturbation of the $\text{B}^3\Pi_{0_u^+}$ crossed by a nonbinding $1_u(1\Pi)$ state (see e.g. [21, 22]) at $E_c \approx 16800 \text{ cm}^{-1}$. This is the only local perturbation accounted for explicitly in the formulas.

The above representation does not explicitly show the dependence on the nuclear moments. No distinction was made yet for including different isotopomers. The extension of the above set of formulae to the case of different isotopomers can be done by splitting off the nuclear moments from the rovibrational representations. The Dunham theory for the rovibrational motion also reveals dependences of the expansion parameters on the reduced mass. For the hyperfine parameters this is not straightforward. We checked the importance of mass corrections and found that within the present data set the results are not influenced by a Dunham-like dependence of the χ_{lk} on the reduced masses. Thus, it is omitted in the formulas given earlier. The energies $E_{v,J}$ are calculated from the Dunham parameters in [23] for the case of $^{127}\text{I}_2$ and are used without mass relations for all isotopomers. \bar{E}_p , $E_{v,J}$ and E_c are referred to $E_{v''=0, J''=0}$ of the ground state.

The isotopic dependence by the nuclear moments is conveniently included by writing the hyperfine parameters χ^i for the isotope i in the following form:

$$\chi^{(i)}(v, J) = \chi^{(\text{ref})} \cdot \gamma_{Q, \mu}^{(i)}, \quad (8)$$

where $\chi^{(\text{ref})}$ is the corresponding parameter for the reference isotopomer $^{127}\text{I}_2$ and $\gamma_Q^i = Q^{(i)}/Q^{(\text{ref})}$ and $\gamma_\mu^i = (\mu^{(i)}/I_1^{(i)})/(\mu^{(\text{ref})}/I_1^{(\text{ref})})$ are the ratios of the nuclear electric quadrupole moments and of the nuclear dipole moments referred to the nuclear spin quantum numbers I_1 . The numerical values are given in table 1.

In this way the numbers given later can be used directly for $^{127}\text{I}_2$ with $\gamma=1$, while for the other isotopomers the factors γ are different from one. These modifications are applied to the nuclear electric quadrupole and the nuclear spin-rotation interaction, where the nuclear moments enter linearly. The nuclear spin-spin interaction is a product of two matrix elements containing a nuclear magnetic moment. So here the square of the ratio, $(\gamma_\mu^{(i)})^2$, must be used.

Finally, we point out that by measuring optical transitions usually (for $J \geq 10$) only differences between the hyperfine parameters of X and B state can be determined, because the corresponding parameters of the two states are strongly correlated, if derived from transitions with selection rules $\Delta F = \Delta J$, which is the case for most of the existing data. By fitting spectra one obtains differences

$$\begin{aligned} \Delta eqQ &= eqQ_B - eqQ_X, \\ \Delta C &= C_B - C_X, \\ \Delta \delta &= \delta_B - \delta_X, \\ \Delta d &= d_B - d_X. \end{aligned} \quad (9)$$

The correlation can be broken, however, if hyperfine structures of low J'' lines are measured,

Table 1. Ratios of nuclear moments used in the fits of the hyperfine parameters.

Nuclear moment	Value	Reference
$\mu^{(127) \text{ a}}$	2.8090(4)	[24]
$\mu^{(129) \text{ a}}$	2.6173(3)	[24]
$\frac{^{129}Q}{^{127}Q}$	0.701213(15)	[25]
$\gamma_\mu^{(127)}$	1	
$\gamma_\mu^{(129)}$	0.6655	
$\gamma_Q^{(127)}$	1	
$\gamma_Q^{(129)}$	0.701213	

^a In units of μ_N (nuclear magneton).

or the signal-to-noise ratio is sufficient to observe the weak $\Delta F = 0$ and $\Delta F = -\Delta J$ transitions, or cross-over resonances of saturation spectroscopy. Such data were included in [4] and are included also in the data sets used here. This makes it possible to distinguish the hyperfine interaction of the upper and the lower electronic state as is done in this paper.

Due to the nuclear spins $I_1 = \frac{5}{2}$ for ^{127}I and $I_1 = \frac{7}{2}$ for ^{129}I , the full hyperfine pattern of a transition with selection rule $\Delta F = \Delta J$ of $^{127}\text{I}_2$ exhibits 15 hyperfine components when J'' is even and 21 when J'' is odd; for $^{129}\text{I}_2$ we have 28 resp. 36 components. Transitions of the mixed isotopomer $^{127}\text{I}^{129}\text{I}$ always have 48 hyperfine components, independent of J'' even or odd. The hyperfine components in the spectra are assigned by labels a_1 to a_n from lower to higher frequencies, n being the maximum number of components depending on J'' even or odd and on the isotopomer.

4. Measurements and results

Spectra from both saturation setups were observed simultaneously, with the issue to cover as many bands as possible in the range supplied by the laser available. In different periods of measurements, ranges around 633 and 612 nm, additionally from 610 to 615 nm and from 573 to 583 nm were recorded and lines of rovibronic bands were observed involving v'' from 0 to 5 and v' from 9 to 20 for all three isotopomers. An example of a simultaneously recorded spectrum is shown in figure 2. As discussed in section 2 the ranges were selected such that in each scan a hyperfine component with a known absolute frequency calibration was included [13, 14]. First, a relative frequency scale was established from the markers of the stabilized Fabry–Pérot cavity by performing a spline-fit and a linearization procedure to the series of markers. Subsequently, this scale was converted into an absolute frequency scale by linking it to one of the hyperfine components known at high accuracy.

Fitting of the hyperfine structures of the transitions was performed by programs, in which the hyperfine codes described in section 3.1 were embedded to create calculated spectra from the list of hyperfine splittings and relative intensities. Each hyperfine component is represented by a standard line shape profile [18] of the form

$$f(x) = \frac{1}{1 + a(x - x_0)^2 + (1 - b - a)(x - x_0)^4 + b(x - x_0)^6} \quad (10)$$

with $x = 2\nu/\Delta\nu$ as a reduced frequency variable and $\Delta\nu$ being the full width at half maximum (FWHM), and $x_0 = 2\nu_0/\Delta\nu$ is the line position. Having calculated a hyperfine pattern by giving values to a , b , FWHM and the hyperfine parameters for each state, additional parameters are necessary for intensity scaling and background of the calculated structure for best coincidence with the observed pattern.

Fitting of the hyperfine parameters is done using the MINUIT package [26], which minimizes the function

$$\chi^2 = \sum_i w_i \cdot (obs_i - calc_i)^2 \quad (11)$$

by adjusting the variable parameters: obs_i is the measured signal at position i , $calc_i$ the corresponding calculated one, w_i is the weight for that data point. The weights are determined by the program from a part of the spectrum with only background, in order to take the signal-to-noise ratio of the measurement into account, and is usually the same for all i . It can be set to zero within a fit for chosen data points to be excluded from the fit. Such an approach was used in cases when the line to be fitted was blended with one or more other transitions.

For all of our measurements, the selection rule $\Delta F = \Delta J$ applies, so that mainly the differences of the hyperfine parameters are significant, as explained in section 3.1. For good starting values, we calculated the ground state hyperfine parameters using the formulas

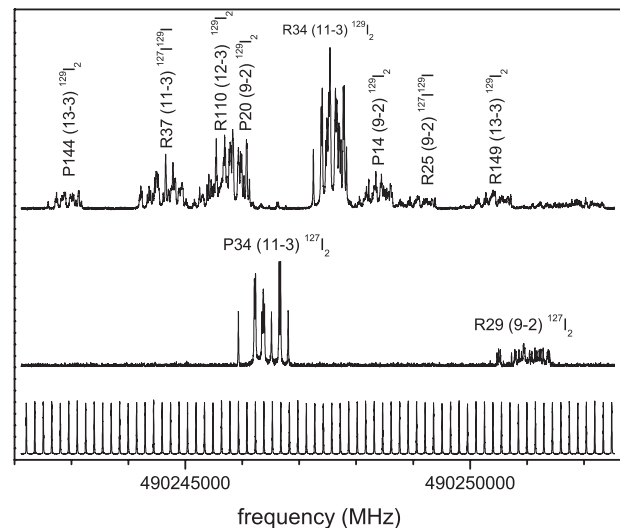


Figure 2. Example of spectra at 611 nm, recorded around P34 (11–3) of $^{127}\text{I}_2$. The lowest trace shows the markers used for the frequency scale, the middle trace is the pure $^{127}\text{I}_2$ spectrum, while the upper trace is from the $^{129}\text{I}_2$ cell and shows in addition lines due to the mixed isotopomer and weak signals from $^{127}\text{I}_2$.

given in [4] with isotopic corrections according to equation (8) and kept them fixed. Moreover, checking the frequency contributions by the nuclear spin–spin interaction to the hyperfine splitting in the range of quantum numbers relevant in our present measurements, they turn out to be less than 400 kHz. This is significantly smaller than the experimental uncertainty of the present experiment, typically about 2 MHz, so we cannot expect any reliable determination of such parameters from our spectra. Therefore, again applying the formulas given in [4] and isotopic corrections we calculated the nuclear spin–spin parameters also for the upper state and kept them fixed for the homonuclear case in all fits, while in the heteronuclear case this interaction was not taken into account at all. Similarly the number of the other parameters could be reduced. It turned out that b of the line shape (equation (10)) is not significant, so it was set to zero. Only the parameters a and FWHM needed to be adjusted, and the intensity scaling and background, and a global frequency shift as well.

For $^{127}\text{I}_2$ we had a fairly long cell available. So the pump beam is attenuated due to Doppler-broadened linear absorption until it crosses with the probe beam. Thus in the peak region of the Doppler broadened line the pump beam is weaker than in the wings, giving less saturation. Also the probe beams are attenuated by the same phenomenon, and this was not fully compensated for in the experimental setup. As can be seen in figure 3, the hyperfine components are sitting on some wider background, and moreover the saturation signals are weaker in the middle of the structure than expected when compared to calculated ones or to the corresponding line in the atlas by Katô *et al.* [2]. For correction of the background of the probe beam a Gaussian function was introduced with a FWHM comparable to the width of the Doppler broadened absorption line. For additional correction of the intensity attenuation of the pump beam another Gaussian function, sharing the parameter centre frequency and FWHM with the background correction of the probe beam, but with an independent intensity factor, was multiplied with the calculated intensities of the hyperfine components. With these additional means good agreement between observed and calculated spectra for $^{127}\text{I}_2$ could be achieved. In figure 3, a transition with even J'' is shown, which exhibits 15 hyperfine components. For the fit in figure 3 all of the above mentioned corrections to background and intensity have been applied. The lower trace displays *obs. – calc.* and one can see small deviations, especially around the component of lowest frequency, while other components fit better. Such behaviour was observed sometimes even more pronounced, and also

for the other isotopomers. We attribute this to slight nonlinearities in the frequency scale, caused by deviations of the laser scan from linearity between two markers separated by 150 MHz, which we cannot correct for.

We checked the effect of the background and intensity correction on the determination of the hyperfine parameters. It is smaller than the scatter of the parameter values derived from different records of the same line, so that any residual effect can be considered as being absorbed by the experimental uncertainty for cases when this correction was not applied. In figure 4 a fit of the R34 (11–3) line of $^{129}\text{I}_2$ is shown. The lower trace shows that the fit is as good as in figure 3. The total extension of the structure is narrower than in the $^{127}\text{I}_2$ case, as the hyperfine interaction is smaller. Here, no frequency-dependent background or intensity corrections were necessary due to the short length of the cell used. An even J'' results in a structure consisting of 28 components, of which not all are resolved. Figure 5 displays the fit of the R37 (11–3) line of $^{127}\text{I}^{129}\text{I}$. Only very slight deviations are shown by the lower trace displaying the residuals from the fit. This structure has 48 components independent of J'' even or odd, which overlap to a large degree, indicating directly the need of line profile fitting for the hyperfine analysis. Again in this case no frequency-dependent background or intensity corrections were applied.

The bands observed in this work cover vibrational levels $8 \leq v' \leq 20$ in the upper state and $0 \leq v'' \leq 5$ in the lower state. The range of the rotational quantum number J'' is from 10 to 150 for the $^{129}\text{I}_2$ isotopomer, while the ranges for $^{127}\text{I}_2$ and $^{127}\text{I}^{129}\text{I}$ are a bit smaller.

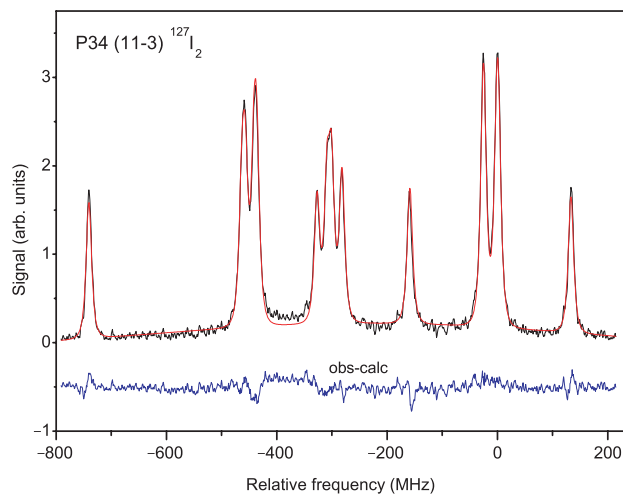


Figure 3. Fit of P34 (11–3) line of $^{127}\text{I}_2$. A difference between observed and calculated spectrum is only obvious around -400 MHz. The lower trace shows the residuals from the fit, shifted down from zero for better visibility.

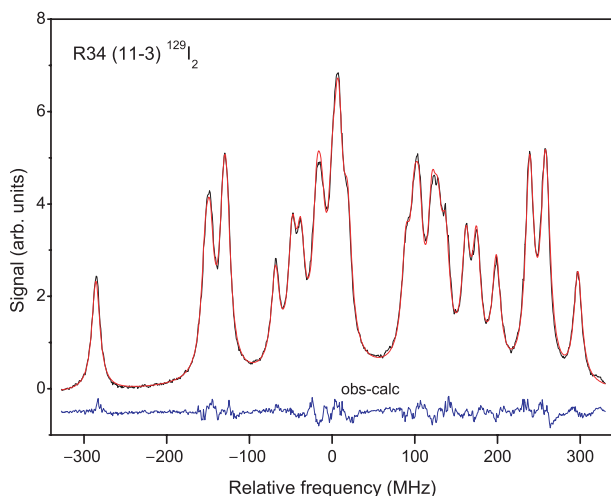


Figure 4. Fit of R34 (11–3) band of $^{129}\text{I}_2$. The lower trace shows the residuals from the fit, shifted down from zero for better visibility.

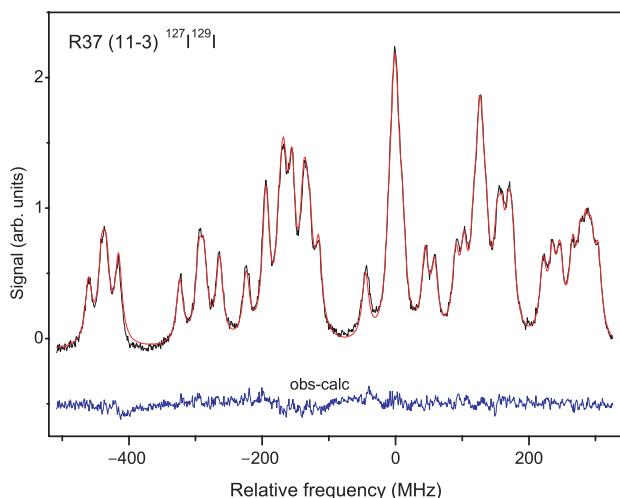


Figure 5. Fit of R37 (11–3) band of $^{127}\text{I}^{129}\text{I}$. The lower trace again indicates the residuals from a fit, shifted down from zero for better visibility.

Altogether, more than 120 eqQ_B parameters of $^{127}\text{I}_2$, more than 200 for $^{129}\text{I}_2$ and more than 170 for $^{127}\text{I}^{129}\text{I}$ have been determined. The same numbers apply to new C_B values.

The tables of the individual hyperfine parameters will not be included here due to their length. The eqQ data are given in part 1 of the electronic supplement [27], while the new data of the spin–rotation parameter C are collected in part 2. The values in the lists are given as ΔeqQ and ΔC according to equations (9), respectively.

When a certain line was recorded more than once, we averaged the resulting eqQ_B and C_B and give the standard deviation as the uncertainty. For hyperfine parameters inferred from single measurements we give

uncertainties which are estimated by comparison with typical cases of the previously described situation of more than one line, according to the signal-to-noise ratio of the experimental spectrum and the quality of the fit, which also accounts for blends with other lines. Typical uncertainties for ΔeqQ are 2 MHz and for ΔC are 2 kHz.

5. Analysis of hyperfine functions

The new data of this paper and recent data from literature [6, 28–31] have been used to derive a set of formulas, describing the rovibrational dependence of the hyperfine parameters. Based on the data given in [4], improved data sets have been established. As far as the original frequencies were given in literature, the hyperfine parameters were refitted using our own hyperfine code.

Usually, we found good agreement with the residuals and the hyperfine parameters given in the original papers. Only in the case of R121 (35–0) of $^{127}\text{I}_2$ given in [29] we found a deviation. We were able to fit all components including a_8 and a_{12} with a reasonable standard deviation of 2.2 kHz. This is in contrast to the fit given in that paper, where these two components show deviations of about +40 MHz and –40 MHz, respectively. These deviations might be an artefact of the program code used there.

The data by Chen *et al.* [6] extend the range of quantum states in the upper state substantially, so they will extend the validity of the models to higher vibrational levels. However, for levels higher than $v' = 55$ perturbations were observed [6], which have been attributed to electronic states sharing the same asymptote as the B state. Actually even for $v' = 42$ and higher levels some irregularities were observed by increased standard deviations of their fits and attributed to local perturbations by the $1_g(1\Pi_g)$ state, but they were still small.

The perturbations cannot be described by our simple models, so for the sake of reliable prediction covering a large range as reference spectra, we prefer to keep some distance from the more heavily perturbed vibrational quantum numbers range. Thus we restrict here the ranges of our description to vibrational levels $0 \leq v'' \leq 17$ for the $X^1\Sigma_g^+$ state and $0 \leq v' \leq 53$ for the $B^3\Pi_{0g^+}$ state.

5.1. Nuclear spin–spin interaction

Several new measurements around 532 nm, all of bands with $32 \leq v' \leq 36$ have been published [28–31], and new data are available for $v' \geq 42$ [6]. From the frequency tables in [11] hyperfine parameters for $^{129}\text{I}_2$ were fitted,

but only the data for the P69 (12–6) line of $^{129}\text{I}_2$ are sufficiently accurate and complete for fitting reliable nuclear spin–spin parameters. These were also introduced to the data set. No parameters from the present measurements were included, because they could not be determined precisely enough. At the expense of two additional parameters for the upper state compared to our previous formulas (remark: erroneously the formulas (12) and (13) in [4] read $\Delta\delta$ and Δd , they should, however read δ_B and d_B), all data up to $v' = 53$ can be described by formulas (6) and (7), using the parameters listed in table 2.

The ground state parameters were not changed, due to lack of new information on the ground state, $\delta_X = 3.705$ kHz, $d_B = 1.524$ kHz are used. The value of δ_B of R30 (42–0) [6] has been excluded from the fit, because due to its different sign compared to the other ones it seems to be perturbed. The data were weighted with their experimental uncertainties, the standard deviation of the fit is 1.6 kHz. To estimate the contributions of the nuclear spin–spin interactions to the total hyperfine splitting, we give rules of thumb for $^{127}\text{I}_2$ here. The contributions of the nuclear spin–spin interaction increase in magnitude with the level energy increasing towards the dissociation limit. While the total contribution to e.g. the component a_2 is 200 kHz for $v' = 11$, it amounts to 1.1 MHz for the same component of P89 (53–0), which is the transition with the highest level in the fit. Similar magnitudes are calculated for a_{20} , while the contribution to a_{13} is about a factor of two less. This applies to the mentioned hyperfine components for odd J'' . For even J'' the corresponding components are a_1 , a_{10} and a_{15} , and the contributions are of similar order. This is the magnitude of error one has to take into account if the interaction is completely neglected, as was done sometimes in literature.

Looking at the fit residuals, despite overall good agreement few larger deviations of about 10 kHz occur. Taking such value as an uncertainty of prediction of $\Delta\delta$ or Δd , the resulting frequency uncertainty would be not larger than 65 kHz for component a_1 (a_2), 25 kHz for a_{10} (a_{13}) and 50 kHz for a_{15} (a_{20}) for even J'' (odd J'') in the range of quantum numbers given above.

5.2. Nuclear spin–rotation interaction

There are the new high precision data from the literature [6, 11, 28–32] and new data from the present measurements. The data set for the fit comprises about 640 C_B and ΔC values of $^{127}\text{I}_2$, $^{129}\text{I}_2$ and $^{127}\text{I}^{129}\text{I}$. For the X ground state no new data exist, so those parameters are unchanged compared to [4], and were kept fixed in the fit. For the upper state we had to introduce two new parameters in the rovibrational dependence of the

terms describing the perturbation from the electronic states sharing the same asymptote with the B state, in order to obtain a convincing fit. The parameters for representations of C_X and C_B due to equation (5) are listed in table 3. In order to give practical estimations of the prediction uncertainties, the sensitivity of different

Table 2. Parameters for representation of δ_B and d_B according to equations (6) and (7) from the combined fit of scalar and tensorial nuclear spin–spin-interaction parameters. For the ground state $\delta_X = 3.705$ kHz, $d_X = 1.524$ kHz are used.

Parameter	Value	Unit
δ_{00}	20.88	kHz
d_{00}	25.93	kHz
$\chi_{00}^{(\Omega=0)}$	39698	kHz/cm $^{-1}$
$\chi_{21}^{(\Omega=0)}$	0.2475×10^{-3}	kHz/cm $^{-1}$
$\chi_{00}^{(\Omega=1)}$	106923	kHz/cm $^{-1}$
$\chi_{21}^{(\Omega=1)}$	0.1712×10^{-3}	kHz/cm $^{-1}$
η_{\perp}	–22.41	kHz
$\bar{E}_{\Omega=0}$	19973	cm $^{-1}$
$\bar{E}_{\Omega=1}$	20534	cm $^{-1}$
E_c	16787	cm $^{-1}$
W	260267	(cm $^{-1}$) 2

Table 3. Parameters for representation of C_X and C_B according to equation (5) from the fit of nuclear spin–rotation-interaction parameters.

Parameter	Value	Unit
$X^1 \Sigma_g^+$		
$\chi_{00}^{(1)}$	1.9245	kHz
$\chi_{10}^{(1)}$	0.01356	kHz
$\chi_{00}^{(p)}$	–15098	kHz/cm $^{-1}$
\bar{E}_p	12340	cm $^{-1}$
$B^3 \Pi_{0_u}^+$		
$\chi_{00}^{(1)}$	28.89	kHz
$\chi_{10}^{(1)}$	0.9234×10^{-1}	kHz
$\chi_{01}^{(1)}$	0.2241×10^{-2}	kHz
$\chi_{11}^{(1)}$	0.1027×10^{-4}	kHz
$\chi_{00}^{(p)}$	36672	kHz/cm $^{-1}$
$\chi_{10}^{(p)}$	–3388	kHz/cm $^{-1}$
$\chi_{01}^{(p)}$	9.7985	kHz/cm $^{-1}$
$\chi_{11}^{(p)}$	–0.2201	kHz/cm $^{-1}$
\bar{E}_p	20140	cm $^{-1}$

hyperfine components to changes of the nuclear spin–rotation interaction parameter was inspected for the main isotopomer $^{127}\text{I}_2$. Least sensitive are components a_1 (a_2), a_{10} (a_{13}) and a_{15} (a_{20}) in the case of even (odd) J'' . The contribution of the spin–rotation interaction increases with v' towards the dissociation limit. However, for P89 (53–0), which involves the highest level in the fit, the total contribution of the nuclear spin–rotation to a_2 is only 1.2 MHz, to a_{13} is 3.2 MHz and for a_{15} we find 6.3 MHz. Taking an experimental uncertainty of 1 kHz for ΔC , even for the lines with highest upper levels a frequency uncertainty amounts to changes of less than 15 kHz for those hyperfine components. Thus, these are recommended for the purpose of calibration. In contrast, the most sensitive components are a_2 (a_1) for even (odd) J'' , where the contribution of the nuclear spin–rotation interaction, e.g. for P89 (53–0), a_1 , is in total 217 MHz.

5.3. Nuclear electric quadrupole interaction

The new high precision data from literature [6, 11, 28–32] have been included in the data set, together with new data from the present investigations, for the fit of the rovibrational dependence of the interaction parameters. To account properly for data with largely different uncertainty, a weighted least squares fit was used. Altogether more than 650 eqQ_X , eqQ_B and ΔeqQ values for all three isotopomers have been included in the new data set. For the upper state we need to introduce two more parameters to cover the extended vibrational range with good accuracy. The ground state parameters were also fitted, which improved the χ^2 of the fit by a factor of two. The results for $eqQ_X(v'', J'')$ and $eqQ_B(v', J')$ are given in table 4. The standard deviation of the fit is 13 kHz, mainly determined by the high precision data. In figure 6, the fit residuals are shown. We have restricted them to the high precision data only for better overview. Most of the data deviate from the fit by less than 0.5 MHz. Two of the measurements by [32] (P78 (1–9), R113 (3–10)) of $^{127}\text{I}_2$ were excluded, as the deviations were about 10 times their claimed accuracy. If the deviations were due to perturbations, they could not be described with our models.

Overall, the fit of eqQ describes the high precision data fairly well. The same applies to the data gathered in this work. For all three isotopomers, they generally agree very well with the model description within their uncertainty limits.

On using the formulas above for prediction of hyperfine splittings, we give an estimation of the

expected prediction uncertainty for $^{127}\text{I}_2$. From the discussion on the nuclear spin–rotation interaction in section 5.2 the hyperfine components a_1 (a_2), a_{10} (a_{12}) and a_{15} (a_{20}) were identified and recommended as

Table 4. Parameters for representation of eqQ_X and eqQ_B according to equation (5) from the fit of the nuclear quadrupole interaction parameters. For the ratios of nuclear quadrupole moments see table 1.

Parameter	Value	Unit
$X^1\Sigma_g^+$		
$\chi_{00}^{(1)}$	−2452.285	MHz
$\chi_{10}^{(1)}$	−0.5474	MHz
$\chi_{20}^{(1)}$	0.4487×10^{-1}	MHz
$\chi_{01}^{(1)}$	-0.2089×10^{-3}	MHz
$\chi_{11}^{(1)}$	0.6965×10^{-5}	MHz
$B^3\Pi_{0g^+}$		
$\chi_{00}^{(1)}$	−488.086	MHz
$\chi_{10}^{(1)}$	−1.83777	MHz
$\chi_{30}^{(1)}$	0.99774×10^{-4}	MHz
$\chi_{50}^{(1)}$	0.80818×10^{-8}	MHz
$\chi_{01}^{(1)}$	-0.14020×10^{-3}	MHz
$\chi_{11}^{(1)}$	-0.32217×10^{-5}	MHz
$\chi_{21}^{(1)}$	0.2716×10^{-7}	MHz
$\chi_{02}^{(1)}$	-0.3377×10^{-9}	MHz

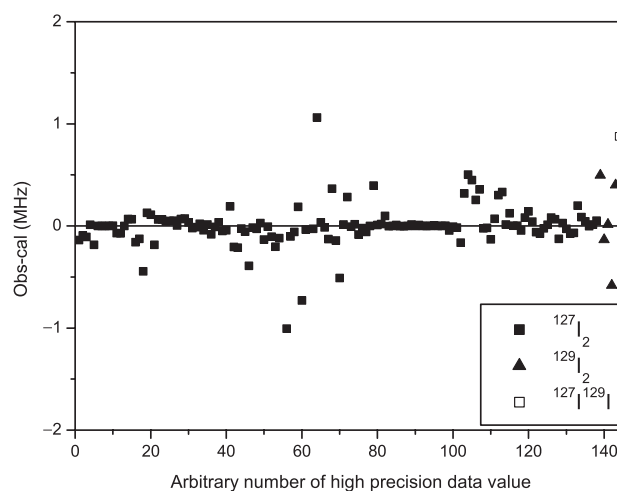


Figure 6. Fit residuals of fit of nuclear electric quadrupole interaction, ordered by number of data value. The values from 76 to 97 correspond to the high precision data from around 532 nm and have the highest weight in the fit.

being least sensitive to uncertainties of ΔC . Out of these, the component a_{10} (a_{12}) for even (odd J'') lines are those with smallest energy contribution by the nuclear electric quadrupole interaction, which is roughly around 100 MHz. Typical values of ΔeqQ are 2000 MHz for $^{127}\text{I}_2$. Thus the uncertainties in the prediction of ΔeqQ will convert to frequency uncertainties of that hyperfine component by dividing by about a factor of 20, and factors of 4 and 5 for a_1 (a_2) and a_{15} (a_{20}). Thus a change of ± 1 MHz of ΔeqQ gives ± 0.25 MHz for a_1 (a_2), ± 0.05 MHz for a_{10} (a_{13}) and ± 0.2 MHz for a_{15} (a_{20}) in the range of vibrational quantum numbers specified.

Combining the uncertainties for the hyperfine interactions, finally an uncertainty of less than 60 kHz can be expected for the prediction of component a_{10} (even J'') resp. a_{13} (odd J''), which is the best one of these recommended for calibration purposes.

6. Discussion and conclusion

The hyperfine structures of rovibronic lines of the $\text{B}^3\Pi_{0^+}-\text{X}^1\Sigma^+$ system of the isotopomers $^{127}\text{I}_2$, $^{129}\text{I}_2$ and $^{127}\text{I}^{129}\text{I}$ have been recorded by saturation spectroscopy. The parameters of the relevant hyperfine interactions have been extracted by combined fits of calculated spectra to the measured ones. The hyperfine parameters obtained have been used together with data known from the literature in models which describe the dependence of the hyperfine parameters on vibration and rotation in both electronic states for all three isotopomers with good precision. The models predict hyperfine parameters which can be used to calculate line positions within a hyperfine pattern. For reference purposes the components a_1 , a_{10} and a_{15} for (even J''), and a_2 , a_{13} and a_{20} for (odd J'') of $^{127}\text{I}_2$ are recommended, because they have only small dependence on the magnetic hyperfine interactions. The uncertainty of those lines is governed by the uncertainty of the description of the nuclear electric quadrupole interaction, and as a rule of thumb will be less than 60 kHz for a_{10} or a_{13} in the case of even J'' or odd J'' . This is sufficiently precise for the prediction of frequencies of hyperfine transitions, which reach few MHz accuracy when combined with appropriate models for the rovibronic structure of the electronic states. Such models will be presented in a future paper. For the isotopomers $^{129}\text{I}_2$ and $^{127}\text{I}^{129}\text{I}$ the prediction uncertainty is less due to only a few high precision measurements being available in the literature. The combined evaluation of all isotopomers with the models presented transfers precision to the other isotopomers. From the fits of the new measurements

presented here, applying similar estimations as before in section 5 for $^{127}\text{I}_2$, we expect a prediction uncertainty of hyperfine splittings of $^{129}\text{I}_2$ and $^{127}\text{I}^{129}\text{I}$ not larger than 1 MHz. This is still sufficiently precise for a total prediction uncertainty of a few MHz for rovibronic transitions including hyperfine structure. A drawback of these isotopomers for use as high reference spectra might be the overlap of many hyperfine components. Only for $^{129}\text{I}_2$ and even J'' , one hyperfine component, a_1 , is sufficiently separated from the other ones to be used as a reference line free from overlap. For calibrations, which do not require highest precision, also the overlapped structures can be used.

Acknowledgements

This study is supported by the European Community, Integrated Infrastructure Initiative action (RII3-CT-2003-506350) and by the Netherlands Foundation for Fundamental Research of Matter (FOM).

References

- [1] S. Gerstenkorn and P. Luc, *Atlas du Spectre d'Absorption de la Molecule d'Iode* (Laboratoire Aimé Cotton, CNRS II, 91405 Orsay, France), 14 000–5 600 cm^{-1} (1978), 15 600–17 600 cm^{-1} (1977), 17 500–20 000 cm^{-1} (1977); S. Gerstenkorn, J. Verges, and J. Chevillard, *Atlas du Spectre d'Absorption de la Molecule d'Iode* (Laboratoire Aimé Cotton, CNRS II, 91405 Orsay, France), 11 000–14 000 cm^{-1} (1982).
- [2] H. Katô, M. Baba, S. Kasahara, K. Ishikawa, M. Misono, Y. Kimura, J. O'Reilly, H. Kuwano, T. Shimamoto, T. Shinano, C. Fujiwara, M. Ikeuchi, N. Fujita, M. H. Kabir, M. Ushino, R. Takahashi, and Y. Matsunobu, *Doppler-Free High Resolution Spectral Atlas of Iodine Molecule* (Japan Society for the Promotion of Science, Japan, 2000).
- [3] H. Knöckel, B. Bodermann, and E. Tiemann, *Eur. Phys. J. D* **28**, 199 (2004).
- [4] B. Bodermann, H. Knöckel, and E. Tiemann, *Eur. Phys. J. D* **19**, 31 (2002).
- [5] Such program is available under the name 'IodineSpec' from TOPTICA Corp. (www.toptica.com).
- [6] L. Chen, W.-Y. Cheng, and J. Ye, *J. Opt. Soc. Am.* **21**, 820 (2004).
- [7] L. Chen, W. A. de Jong, and J. Ye, *J. Opt. Soc. Am.* **22**, 951 (2004).
- [8] D. Cerny, R. Bacis, and J. Verges, *J. Molec. Spectrosc.* **116**, 458 (1986).
- [9] G. W. King, I. M. Littlewood, J. R. Robbins, and N. T. Wijeratne, *Chem. Phys.* **50**, 291 (1980).
- [10] M. Tesic and Y. H. Pao, *J. Molec. Spectrosc.* **57**, 75 (1975).
- [11] T. J. Quinn, *Metrologia* **40**, 103 (2003).

- [12] M. Klug, K. Schulze, U. Hinze, A. Apolonskii, E. Tiemann, and B. Wellegehausen, *Opt. Commun.* **184**, 215 (2000).
- [13] I. Velchev, R. van Dierendonck, W. Hogervorst, and W. Ubachs, *J. Molec. Spectrosc.* **187**, 21 (1998).
- [14] S. C. Xu, R. van Dierendonck, W. Hogervorst, and W. Ubachs, *J. Molec. Spectrosc.* **201**, 256 (2000).
- [15] R. K. Raj, D. Bloch, J. J. Snyder, G. Camy, and M. Ducloy, *Phys. Rev. Lett.* **44**, 1251 (1980).
- [16] J. J. Snyder, R. K. Raj, D. Bloch, and M. Ducloy, *Opt. Lett.* **5**, 163 (1980).
- [17] M. Broyer, J. Vigué, and J. C. Lehmann, *J. Phys. (France)* **39**, 591 (1978).
- [18] H. Knöckel, S. Kremser, B. Bodermann, and E. Tiemann, *Z. Phys. D* **37**, 43 (1996).
- [19] K. F. Freed, *J. Chem. Phys.* **45**, 1714 (1966).
- [20] V. Spirko and J. Blabla, *J. Molec. Spectrosc.* **129**, 59 (1988).
- [21] J. Tellinghuisen, *J. Chem. Phys.* **57**, 2397 (1972).
- [22] J. Vigué, M. Broyer, and J. C. Lehmann, *J. Phys. (France)* **42**, 937 (1981).
- [23] S. Gerstenkorn and P. Luc, *J. Phys. (France)* **46**, 867 (1985).
- [24] H. Walchli, R. Livingston, and G. Hebert, *Phys. Rev.* **82**, 97 (1951).
- [25] R. Livingston and H. Zeldes, *Phys. Rev.* **90**, 609 (1953).
- [26] F. James and M. Roos, D506 Minuit (Cern Library PACKLIB, 1989).
- [27] Supplementary data files deposited in the archive of *Molecular Physics*; Part 1 contains information on the nuclear spin-rotation coupling constants C_B and C_X ; Part 1 contains information on the electric quadrupole coupling constants eQq_B and eQq_X .
- [28] F.-L. Hong, J. Ishikawa, A. Onae, and H. Matsumoto, *J. Opt. Soc. Am. B* **18**, 1416 (2001).
- [29] F.-L. Hong, Y. Zhang, J. Ishikawa, A. Onae, and H. Matsumoto, *Opt. Commun.* **212**, 89 (2002).
- [30] F.-L. Hong, Y. Zhang, J. Ishikawa, A. Onae, and H. Matsumoto, *J. Opt. Soc. Am. B* **19**, 946 (2002).
- [31] F.-L. Hong, S. Diddams, R. Guo, Z.-Y. Bi, A. Onae, H. Inaba, J. Ishikawa, K. Okumura, D. Katsuragi, J. Hirata, T. Shimizu, T. Kurosu, Y. Koga, and H. Matsumoto, *J. Opt. Soc. Am. B* **21**, 88 (2004).
- [32] P. Dubé and M. Trinczek, *J. Opt. Soc. Am. B* **21**, 1113 (2004).